

## Graphene Aerogels for Ultrabroadband Thermoacoustics

Francesco De Nicola<sup>1,2,\*</sup>, Stefano Sarti,<sup>2</sup> Bing Lu,<sup>3</sup> Liangti Qu,<sup>3</sup> Zhipan Zhang,<sup>3</sup>  
Augusto Marcelli<sup>3,4,5</sup> and Stefano Lupi<sup>1,2</sup>


<sup>1</sup>*Graphene Labs, Istituto Italiano di Tecnologia, Via Morego 30, 16163 Genoa, Italy*

<sup>2</sup>*Department of Physics, University of Rome La Sapienza, Piazzale Aldo Moro 5, 00185 Rome, Italy*

<sup>3</sup>*Beijing Institute of Technology, 100081 Beijing, China*

<sup>4</sup>*INFN – Laboratori Nazionali di Frascati, Via Enrico Fermi 40, 00044 Frascati, Italy*

<sup>5</sup>*RICMASS, Rome International Center for Materials Science Superstripes, Via dei Sabelli 119A, 00185 Rome, Italy*

 (Received 4 March 2020; revised 10 June 2020; accepted 15 July 2020; published 10 August 2020)

Sound is usually generated in a medium by an electromechanical vibrating structure. The geometrical size and inertia of the structure set the frequency cutoff in the sound-transduction mechanism and, often, different vibrating structures are necessary to cover the whole range from infrasound to ultrasound. An alternative mechanism without any physical movement of the emitter is the thermoacoustic effect, where sound is produced by Joule heating in a conductive material. Here we show that a single thermoacoustic transducer based on a graphene aerogel can emit ultrabroadband sound from infrasound (1 Hz) to ultrasound (20 MHz), with no harmonic distortion. Since conventional acoustic transducers are frequency band limited due to their transduction mechanism, ultrabroadband graphene aerogels may offer a valid alternative to conventional hi-fi loudspeakers, and infrasound and ultrasound transducers.

DOI: [10.1103/PhysRevApplied.14.024022](https://doi.org/10.1103/PhysRevApplied.14.024022)

### I. INTRODUCTION

Modern wireless communication is based on transmitting and receiving electromagnetic waves that span a wide frequency range, from hertz to terahertz, providing a large spectral interval for high data-transfer rates. There are drawbacks in electromagnetic communication, though, including a high extinction coefficient for electrically conductive materials and the large size of antennas [1].

However, animals have effectively used acoustic waves for short-range communication for millions of years [2]. Acoustic wave-based communication, although embodying a reduced spectral band due to the geometrical size and inertia of the vibrating structure that set the frequency cutoff in the sound-transduction mechanism [3], can overcome some of the difficulties in electromagnetic wave-based communication and complement existing wireless technologies. For example, acoustic waves propagate well in conductive materials, and thus have been explored for underwater communication (sonar) [4]. Animals such as rodents, bats, and cetaceans are known to communicate and move (ecolocalization) effectively by use of ultrasound waves (20–300 kHz) [2]. In land-based acoustic

wave communication, the audible band (20 Hz to 20 kHz) [3] is often occupied by human conversations and acoustic loudspeakers, whereas the infrasonic band (below 20 Hz) can be disturbed by moving vehicles and building construction [5]. Although infrasonic waves are usually annoying for humans and animals, brain waves (1–600 Hz) occur in this spectral band [6]. Despite having a wide frequency range and often being free of disturbance, the ultrasonic band is rarely used for high-data-rate communication purposes. One possible reason for this is the lack of wide-bandwidth ultrasonic emitters and receivers. Conventional ultrasound transducers [7] exploit the piezoelectric effect, and thus they operate only near their resonance frequencies due to their membrane vibrations. Another typical issue for acoustic transducers is the frequency-dependent impedance of the materials used, which contributes to limit their spectral band [3]. As a result, there is no broadband acoustic transducer to date that covers from infrasound to ultrasound, preventing the broadband or multiband transmission and detection of signals for communications.

An alternative mechanism for sound transduction is the thermoacoustic (TA) effect [2,8–22], where sound is emitted without moving parts by Joule heating when an electric current flows in a conductive material. The root-mean-square sound pressure amplitude  $p_{\text{rms}}$  of a TA wave can be

\*francesco.denicola@iit.it

derived by a general analytical solution of the TA model [23,24] as follows:

$$p_{\text{rms}} = \frac{Rv_g q_0}{\sqrt{2}r_0 C_{p,g} T_g} \frac{e_g}{M(f)e_s + e_g} \mathcal{D}(\theta, \phi), \quad (1)$$

where  $R = Sf/v_g$  is the Rayleigh factor, with  $S$  the emitting surface area of the material,  $f$  the sound frequency, and  $v_g$  the speed of sound in the medium,  $q_0 = Q_0/S$  is the oscillating power density at frequency  $f$  dissipated by the material, with  $Q_0 = |V_i|^2/|Z|$  the amplitude of the oscillating component of the electric power, with  $V(t) = V_0 \sin(2\pi ft)$  the applied ac voltage and  $Z$  the material electrical impedance,  $r_0$  is the far-field distance from the sound source,  $e_i = \sqrt{k_i \rho_i C_{p,i}}$  is the thermal effusivity of the material ( $i = s$ ) and the medium ( $i = g$ ), with  $k_i$  the thermal conductivity,  $\rho_i$  the mass density, and  $C_{p,i}$  the specific heat capacity at constant pressure,  $T_g$  is the medium temperature,  $M(f) \approx 1$  is a frequency-dependent factor, and  $\mathcal{D}(\theta, \phi)$  is the far-field directivity. From Eq. (1) it is evident that the TA effect is not limited in frequency, potentially enabling broadband TA transducers.

Here we introduce a transducer based on a graphene aerogel able to generate ultrabroadband sound from 1 Hz up to 20 MHz by the TA effect. The sound emitted has no observable harmonic distortion in the whole frequency range investigated, and the aerogels act as an omnidirectional point source up to 20 kHz. Furthermore, we demonstrate that, among the other TA transducers [13], graphene has the advantage of having a constant electrical impedance from dc up to the megahertz range, allowing no frequency cutoff or specific resonances, unlike in conventional acoustic transducers [3]. The present research represents a breakthrough for audio consumer technologies, underwater communication [4], transducers for zoological [2] and biomimetic [25] applications, and devices for medical diagnostics [26] and food quality control [27].

## II. EXPERIMENT

### A. Graphene aerogel fabrication

The aerogels are obtained from a graphene oxide dispersion (60 ml, 4–9 mg/ml) and 7 ml of Tween 80 (150 mg/ml) ethanol solution mixed at 2500 revolutions/min for 5 min. The mixture is exposed to liquid nitrogen for 30 min. After freeze-drying for 72 h, the mixture is heated at 300 °C for 2 h in an Ar atmosphere.

The graphene aerogels are cylindrical with diameter  $d = 4$  cm, thickness  $L = 6.5$  cm, and mass  $m = 500$  mg, and therefore have mass density  $\rho_s = 6$  kg/m<sup>3</sup>. From the scanning-electron-microscopy micrograph of a representative sample in Fig. 1(a), it is possible to observe a porous (approximately 80%) random network made of graphene flakes constituting the aerogel surface.

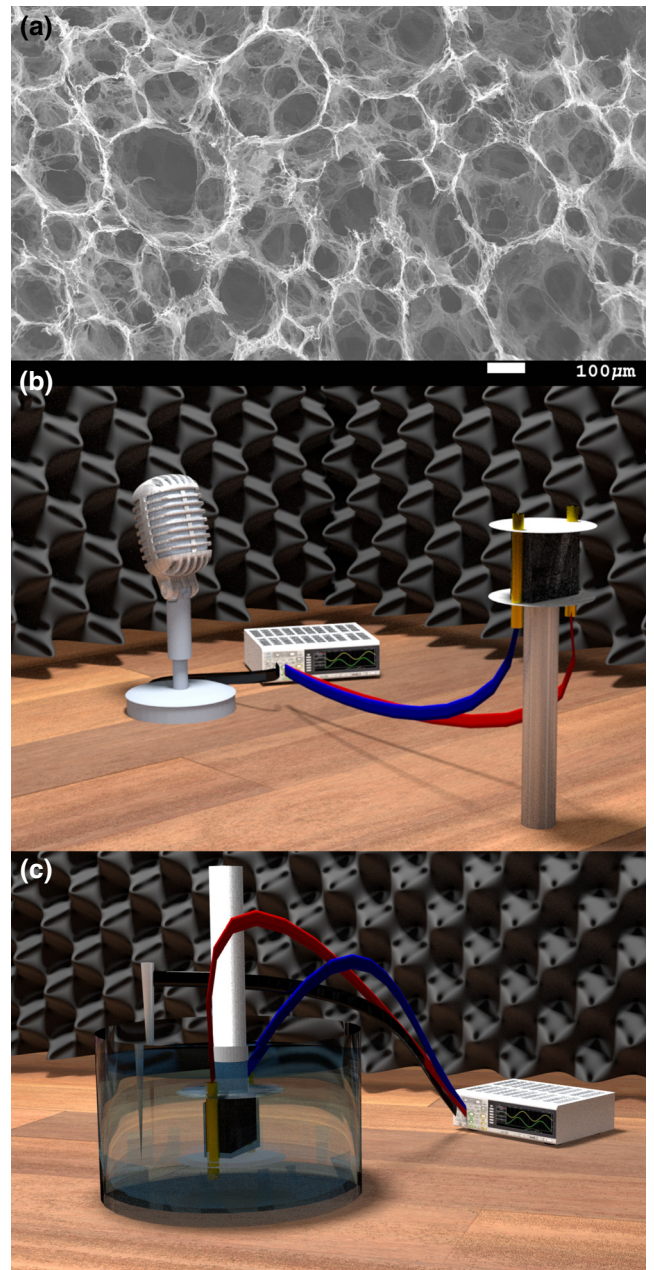


FIG. 1. Graphene-aerogel TA transducers. (a) Representative scanning-electron-microscopy micrograph of a graphene aerogel. (b) Conceptual scheme of the experiment in air. An ac voltage is applied to a graphene-aerogel sample. The sound emitted by the aerogel is recorded by a microphone connected to a sound card. (c) Conceptual scheme of the experiment in water. An ac voltage is applied to a sample placed in a beaker filled with water. The sound emitted by the aerogel is detected by a needle hydrophone immersed in the water and placed at a given angle with respect the sound-emitting surface of the aerogel. The hydrophone output is preamplified by a preamplifier and the hydrophone is connected to a dc coupler and an oscilloscope.

### B. Acoustic characterization

The experimental setup is placed in a soundproof room ( $3 \times 2 \times 2$  m) to acoustically insulate the experimental



apparatus from environmental noise and to reduce internal sound reflections. The audio-signal flow is calibrated in an anechoic chamber at the Italian National Institute for Insurance against Accidents at Work (INAIL).

We measure the acoustic emission of graphene aerogels both in air and in water to avoid ultrasound ( $f > 20$  kHz) absorption by air. The experimental setups in air and in water are shown in Figs. 1(b) and 1(c), respectively. For infrasound and acoustic measurements, a sine-wave voltage signal at a frequency of 1 Hz to 20 kHz is generated by the personal-computer program Room EQ Wizard connected to an RME Fireface UFX sound card. The ac voltage is applied in series to a dc bias at the electrodes connected to the graphene aerogel, and the sound generated at a frequency of 1 Hz to 20 kHz is acquired by a calibrated microphone (Earthworks M50) connected to the sound card and placed in front of the sample at a fixed distance of  $r_0 = 1$  cm for near-field measurements and  $r_0 = 1$  m for far-field measurements. Gated measurements [5] are performed to record the sample sound-frequency response without any sound reflections, as in an anechoic chamber.

For ultrasound measurements, a liquid medium (deionized water  $18 \text{ M}\Omega \text{ cm}$ ) is used to avoid ultrasound absorption by air. A sine-wave voltage signal at a frequency of 20 kHz to 20 MHz is generated by a GFG-8210 function generator. The ac voltage is applied in series to a dc voltage at the electrodes connected to the graphene aerogel immersed in a beaker filled with water, and the sound generated at a frequency of 20 kHz to 20 MHz is acquired by a calibrated 0.2-mm needle hydrophone (Precision Acoustics) connected to a preamplifier, a dc coupler, and an oscilloscope. Since graphene aerogels are superhydrophobic [28], the samples do not absorb water when immersed, and therefore their mass density does not increase.

Directivity patterns are measured by a goniometric stage with the sample fixed in the center and the microphone rotating around the sample.

The sample dynamic range acquired as a function of the sound frequency is divided by the background noise of the room and smoothed at 1/3 per octave. Therefore, here the sound pressure level (SPL) corresponds to the signal-to-noise ratio.

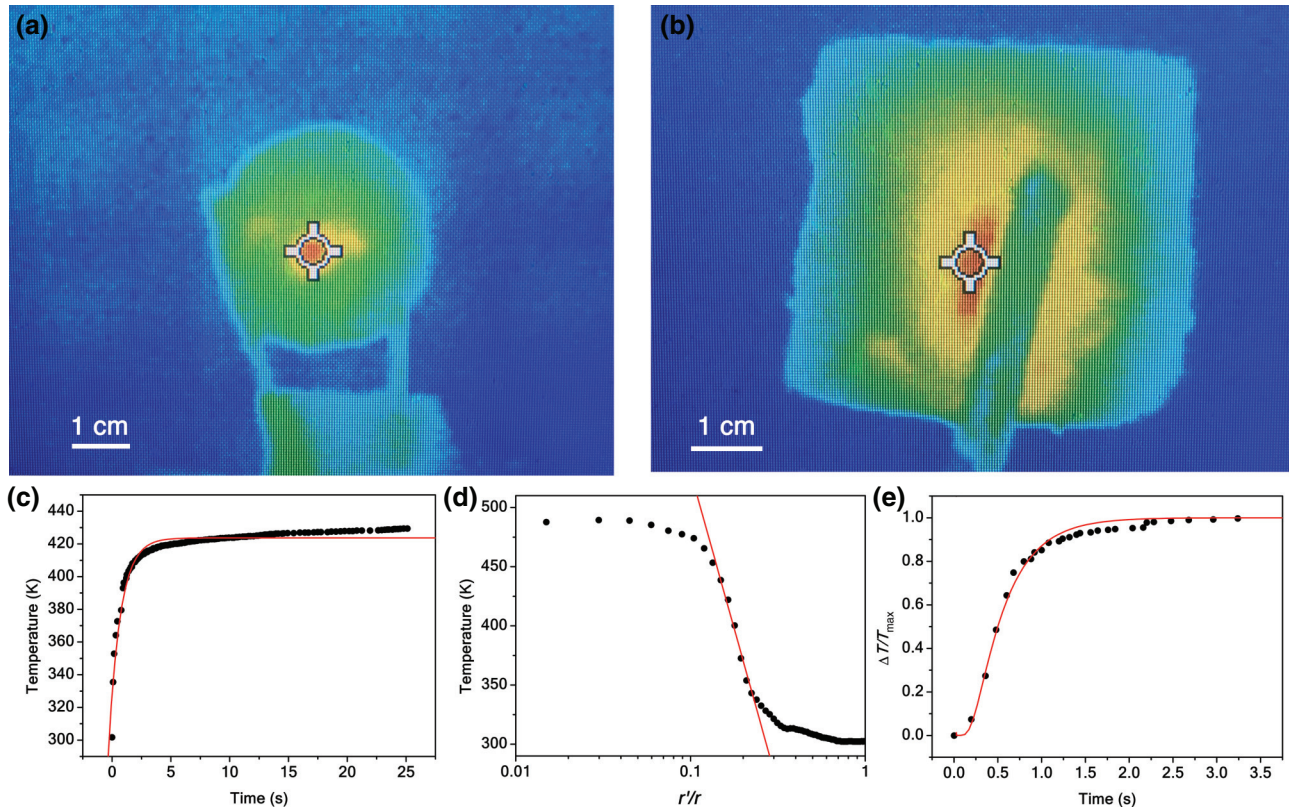


FIG. 2. (a) Thermal-profile image of the heated sample base surface. (b) Thermal-profile image of the heated sample lateral surface. (c) Temperature rise as a function of time on the axis of the graphene aerogel. The data are fit by Eq. (2) (solid red line). (d) Radial thermal profile of the graphene-aerogel illuminated surface as a function of the relative coordinate. The data are fit by Eq. (3) (solid red line). (e) Temperature rise as a function of time at distance  $L$  from the graphene-aerogel heated surface. The data are fit by Eq. 4 (solid red line).

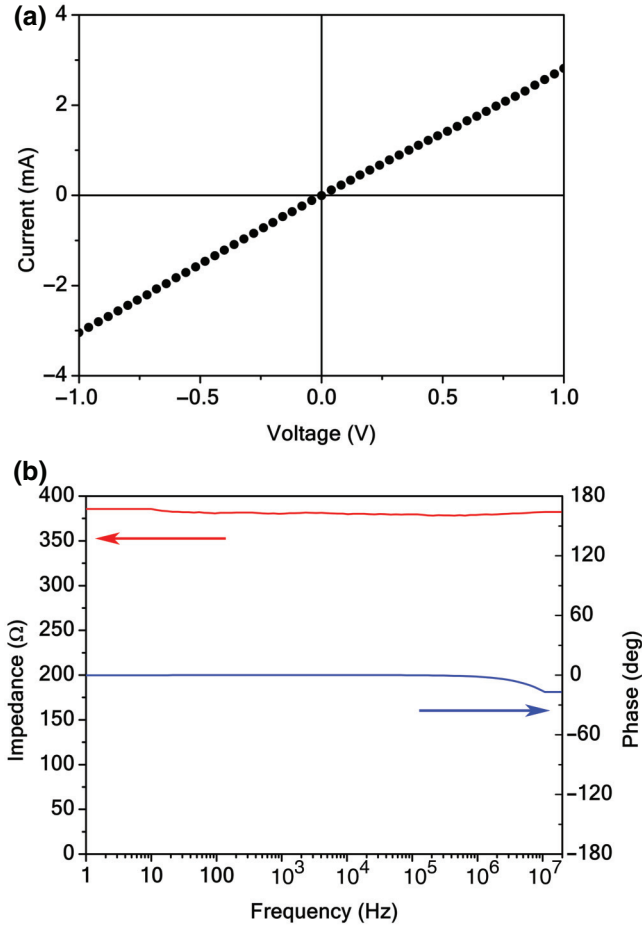


FIG. 3. (a) Electrical current as a function of voltage applied to a graphene aerogel. (b) Modulus and phase of the electrical impedance of a graphene aerogel as a function of frequency.

### C. Thermal characterization

The graphene-aerogel thermal properties are investigated with a Fluke Ti20 thermal camera [Figs. 2(a) and 2(b)]. A sine-wave voltage signal  $V(t) = V_0 \sin(2\pi ft)$  with peak amplitude  $V_0 = 1$  V, frequency  $f = 1$  kHz, and power  $Q = V^2(t)/Z \equiv V_0^2[1 + \cos(4\pi ft)]/2Z$ , with  $Z = 380 \Omega$  the modulus of the electrical impedance of the graphene aerogel, is generated by a GFG-8210 function generator. The ac voltage is applied in series to a  $V_{dc} = 20V_0$  dc bias at the electrodes connected to the graphene aerogel. In this way, the first-harmonic sound generation is recovered by heterodyning [22] with an intensity 80 times higher than the second harmonic, which means a total harmonic distortion [5] of about 1%. However, we could not observe such a small harmonic distortion. Therefore, the power reads  $Q \equiv [(V_0^2 + 2V_{dc}^2) + 4V_0V_{dc} \cos(2\pi ft) + V_0^2 \cos(4\pi ft)]/2Z = 1$  W. It is worth noting that in the thermoacoustic effect only the oscillating component  $Q_0 = [4V_0V_{dc} \cos(2\pi ft) + V_0^2 \cos(4\pi ft)]/2Z$  of the electrical heat  $Q$  contributes to the sound pressure generation.

Heat is provided to the graphene aerogel by the Joule effect, by two electrodes placed at the lateral surface of the cylindrical sample. In a first approximation, heat is dissipated into the aerogel by conduction and in the environment by natural convection and radiation. In particular, by solving the Fourier law of heat in cylindrical coordinates, we find in the cylindrical sample the heat dissipated by conduction is  $Q_{\text{cond}} = 4\pi Lk_s(1 - r'^2/r^2)^{-1}[T(r') - T_s]$ , with  $k_s$  the aerogel thermal conductivity,  $T(r')$  the radial temperature in the sample with radius  $r = 2$  cm, and  $T_s$  the temperature on the sample surface. At the aerogel surface the heat dissipated by radiation equals the heat dissipated by convection  $Q_{\text{rad}} = Q_{\text{conv}}$ , where  $Q_{\text{rad}} = \epsilon\sigma S(T_s^4 - T_g^4)$ , with  $\epsilon = 0.99$  the aerogel emissivity,  $\sigma = 5.67 \times 10^{-8}$  W/m<sup>2</sup>K<sup>4</sup> the Stefan-Boltzmann constant,  $S = 81.6$  cm<sup>2</sup> the aerogel lateral surface, and  $T_g$  the temperature of the medium, and  $Q_{\text{conv}} = hS(T_s - T_g)$ , with  $h$  the natural convection coefficient. Therefore,  $h = \epsilon\sigma(T_s^4 - T_g^4)/(T_s - T_g)$ , which we estimate for air is approximately 6 W/m<sup>2</sup>K and for water is approximately 200 W/m<sup>2</sup>K [29].

The heat-up phase is recorded to obtain the heat capacity  $C_s$  of the samples [Fig. 2(c)]. Since the Debye temperature  $\Theta_D$  of carbon allotropes is approximately 2100 K [30], the heat capacity is not constant in the temperature range considered. Therefore, since the steady state is the one that contributes to the sound generation, we take into account the heat capacity  $C_s = 10^{-1} \pm 10^{-2}$  J/K obtained by our fitting data by the law

$$T(t) = T_{\text{max}} + (T_{\text{min}} - T_{\text{max}}) \exp[(t_0 - t)/\tau], \quad (2)$$

where  $\tau = C_s(T_{\text{max}} - T_{\text{min}})/Q$ ,  $t_0$  is the initial time, and  $T_{\text{max}}$  and  $T_{\text{min}}$  are the sample maximum and minimum temperature measured, respectively.

The thermal conductivity  $k_s$  of the samples is derived by a thermal-profile image of the heated sample base surface at the steady state [Fig. 2(d)] by our fitting the data with the expression

$$T(r') = \frac{Q}{4\pi Lk_s} \left(1 - \frac{r'^2}{r^2}\right) + T_s. \quad (3)$$

The fit returns  $k_s = 10^{-1} \pm 10^{-2}$  W/m K.

Furthermore, since the Biot number  $\text{Bi} \equiv hV/Sk_s = 0.6 > 0.1$ , with  $V = 81.6$  cm<sup>3</sup> the aerogel volume, this suggests a non-negligible internal thermal resistance of the graphene aerogel.

The thermal diffusivity  $\alpha_s$  of the samples is studied by our heating the samples on the base surface and recording the heat-up phase on the orthogonal lateral surface

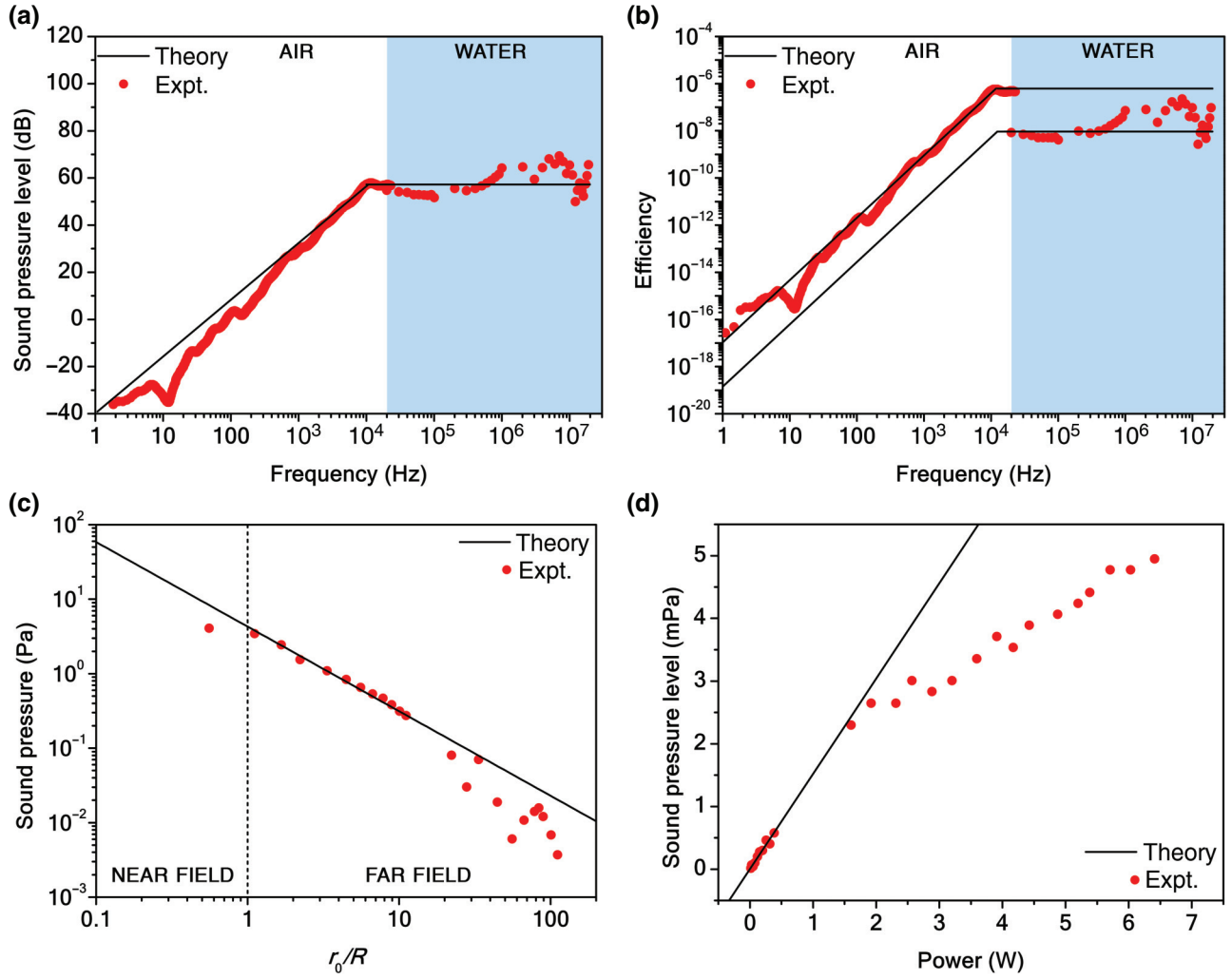


FIG. 4. Thermoacoustic effect in graphene aerogels. (a) Unweighted SPL frequency response at 1 W and 1 m for a graphene aerogel (solid red dots). The solid black curve represents the limiting analytical TA model with no free parameters. (b) Unweighted TA-efficiency frequency response at 1 W and 1 m for the aerogel (solid red dots). The solid black curve represents the TA model. (c) Sound pressure in air at 20 kHz and 1 W as a function of the distance from the graphene-aerogel sound-emitting surface on a log-log scale (solid red dots). The black curve represents the TA model  $p_{\text{rms}} \propto R/r_0$ , which accounts for the far-field regime. The boundary between the near-field regime and the far-field regime is set by the Rayleigh criterion for  $r_0/R = 1$ . (d) Sound pressure in air at 20 kHz/m as a function of the electrical power amplitude (solid red dots). The black curve represents the TA model  $p_{\text{rms}} \propto Q_0$  in the linear regime.

[Fig. 2(e)]. The data are fit by the law [31]

$$T(t) = T_{\text{max}} \left[ 1 + 2 \sum_{n=1}^{\infty} (-1)^n \exp\left(\frac{-n^2 \pi^2 \alpha_s t}{L^2}\right) \right], \quad (4)$$

and we obtain  $\alpha_s = 10^{-4} \pm 10^{-5} \text{ m}^2/\text{s}$ .

Therefore, the minimum effusivity achieved for the samples is  $e_s \equiv \sqrt{k_s \rho_s C_{p,s}} = 10.95 \pm 0.03 \text{ W s}^{1/2}/\text{m}^2 \text{ K}$ , which is larger than the value reported for air ( $6 \text{ W s}^{1/2}/\text{m}^2 \text{ K}$ ) [29] but is lower than the value reported for water ( $1588 \text{ W s}^{1/2}/\text{m}^2 \text{ K}$ ) [29].

#### D. Electrical characterization

Current-voltage curves [Fig. 3(a)] are measured with a Keithley 2612B digital SourceMeter. Impedance measurements [Fig. 3(b)] are conducted with an Agilent HP4192A impedance analyzer.

### III. RESULTS AND DISCUSSION

In Fig. 4(a), the frequency response of the SPL [5]  $L_p = 20 \log_{10}(p_{\text{rms}}/p_0)$ , with  $p_0 = 20 \mu\text{Pa}$  the root-mean-square pressure of the minimum audible threshold, at an input power of 1 W and rescaled to 1 m distance from the

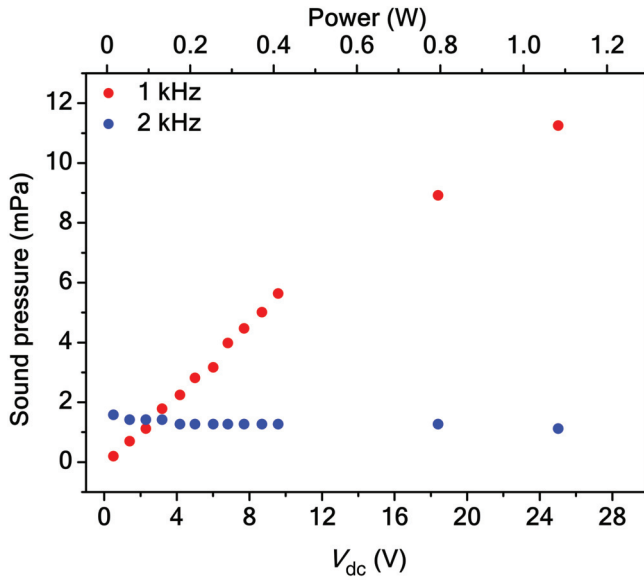


FIG. 5. Sound pressure recorded in air at 1-m distance as a function of dc voltage  $V_{dc}$  applied to the sample with the ac voltage set to  $V_0 = 9$  V, for the first harmonic (1 kHz) and the second harmonic (2 kHz) generated by an input electrical signal of 1 kHz.

source in air and water, according to the Audio Engineering Society standard for acoustic measurements (AES02-1984-r2003) for a graphene aerogel with mass density  $\rho_s = 6.55 \pm 0.01$  is shown. The SPL curves measured in air and water overlap with each other, as the product of the specific heat and the effusivity term is similar for the two media. Furthermore, below 200 Hz, where the modal resonances due to the finite size of the soundproof room reduce the signal-to-noise ratio, the experimental data depart from the TA analytical model with no free parameters in Eq. 1. Also, unlike conventional acoustic transducers [3], the SPL frequency response of graphene aerogels is not dependent on the electrical impedance of the load as the latter is constant in frequency range investigated (see Sec. II). Moreover, owing to the far-field directivity  $\mathcal{D}(\theta, \phi) \propto f^{-1}$  in the ultrasound range, the SPL saturates above 20 kHz at about 60 dB, corresponding to a sensitivity [5] (i.e., the SPL relative to the maximum audible threshold of 120 dB) of  $-60$  dB, which is well above the minimum audible threshold ( $-120$  dB) [5], and is the highest value reported for any TA devices in the ultrasound range [2,32]. For instance, at 20 kHz, 1 W, and 1 cm or at 20 kHz, 1 kW, and 1 m the sensitivity is 0 dB. The graphene-aerogel sensitivity may be increased further by increasing its surface area. In this way, the sound emitted by every point on the aerogel surface heated by the Joule effect coherently adds up to increase the SPL. By comparison, commercial earphones have a similar sensitivity in air as graphene aerogels at 1 W, 1 m, and 1 kHz due to their similar surface area [10]. On the other hand, graphene aerogels act as a highly damped transducer

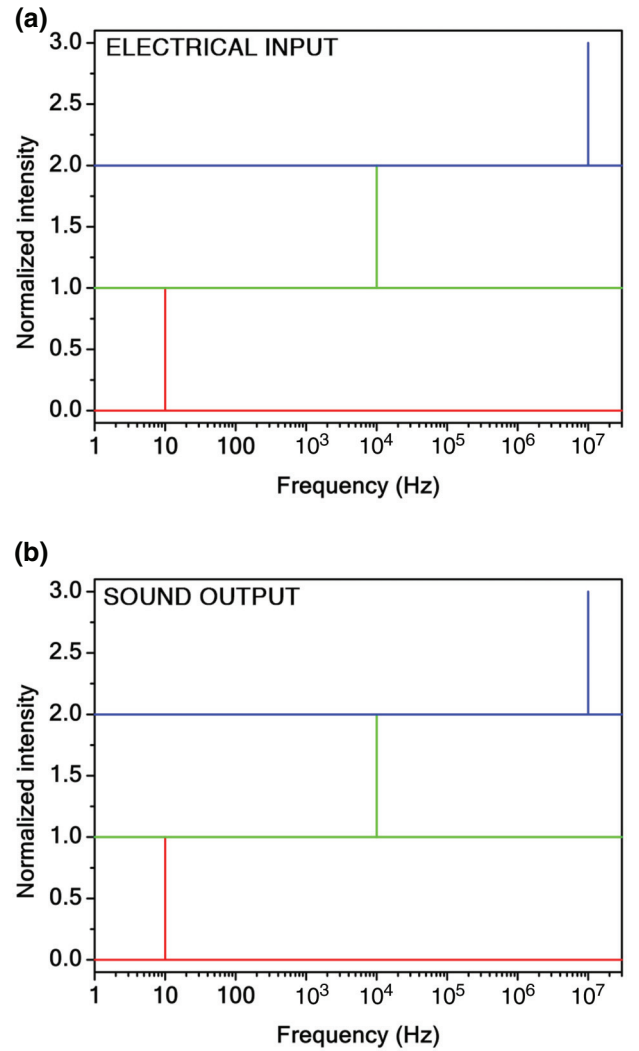


FIG. 6. Harmonic analysis of TA sound emission in graphene aerogels. Fast Fourier transform of the electrical input (a) and sound output (b) signals at 10 Hz, 10 kHz, and 10 MHz. The input and output signals are undistorted from the infrasound region to the audible region, and up to the ultrasound range investigated.

in the ultrasound range [7]. Therefore, graphene aerogels could be successfully used as TA broadband transducers.

According to the TA model [24], the TA efficiency (i.e., the ratio between the output acoustic power  $P_{acous}$  and the input electrical power  $Q_0$ ) reads

$$\eta = \frac{I}{Q_0} r_0^2 \int_0^{2\pi} \int_0^{\pi/2} \mathcal{D}^2(\theta, \phi) \sin \theta d\theta d\phi, \quad (5)$$

where  $I = p_{rms}^2 / \rho_g v_g$  is the sound intensity, with  $\rho_g$  the mass density of the medium. In Fig. 4(b), the TA efficiency at 1 W and 1 m measured in air and water for the graphene aerogel along the theoretical curves is reported. The TA efficiency saturates in the ultrasound range at about  $10^{-7}$



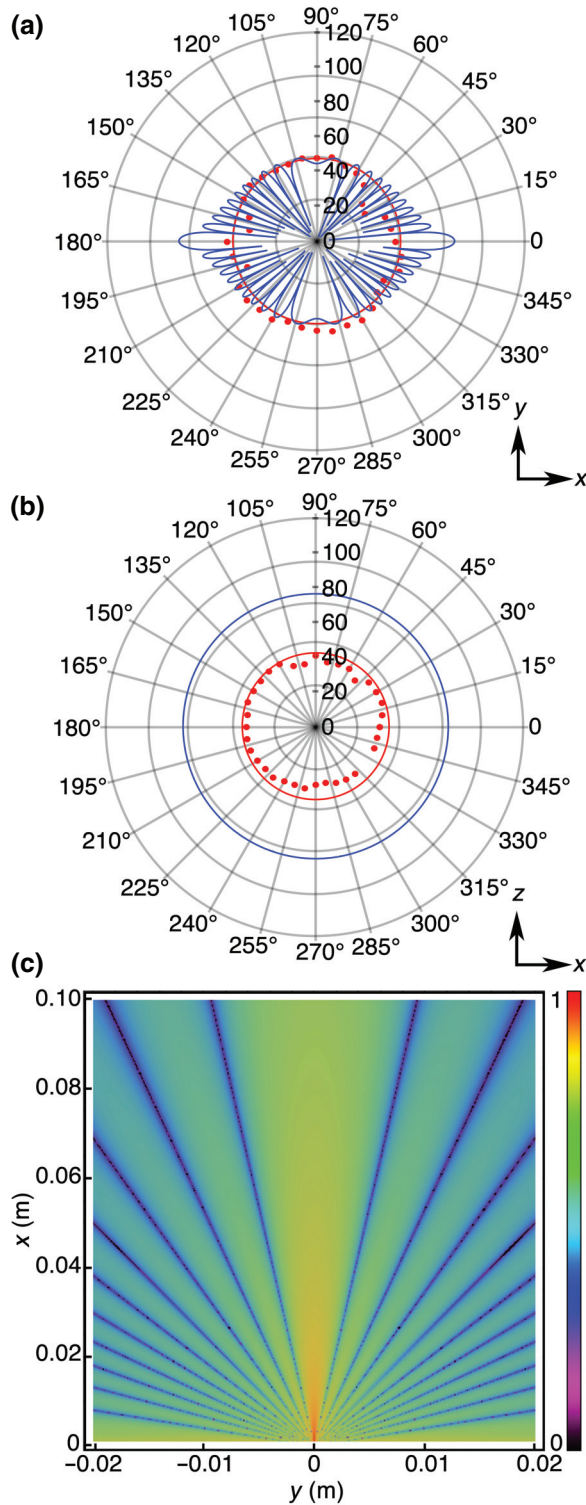


FIG. 7. Thermoacoustic directivity in graphene-aerogel transducers. Experimental sound pressure level at 20 kHz, 1 W, and 1 m as a function of the angle in the azimuthal (a) and polar (b) planes (red dots). The TA model is reported at 20 kHz (solid red curve) and 1 MHz (solid blue curve). The directivity indexes [3] are  $D_i(20 \text{ kHz}) = 11 \text{ dB}$  and  $D_i(1 \text{ MHz}) = 40 \text{ dB}$ . (c) Sound pressure level in space at 1 MHz, 1 W, and 1 m in the azimuthal plane calculated by the TA model. The sound pressure level is normalized to its maximum value.

in air and  $10^{-9}$  in water due to the directivity integral, which is proportional to  $f^{-2}$ . On the other hand, the thermodynamic efficiency of the TA process  $\eta' \equiv 1 - T_c/T_h = 30\%$  is given by a Carnot cycle [13,23] between two heat reservoirs of temperature  $T_c = 298 \text{ K}$  and  $T_h = 430 \text{ K}$ . Evidently 70% of the heat provided to the aerogel is lost in the environment (20% radiatively, 20% convectively, and 30% owing to the sample internal thermal resistance  $R_i \equiv 1/h_i S = 433 \text{ K/W}$ ) without generation of sound.

In Fig. 4(c), we show that the experimental sound pressure at 20 kHz at 1 W departs from the far-field TA model for  $r_0/R < 1$ , in agreement with the Rayleigh criterion that defines the boundary between the near-field regime and the far-field regime [33]. In addition, Fig. 4(d) illustrates that for values of electrical power  $Q_0 > 1.5 \text{ W}$  the experimental sound pressure at 20 kHz and 1 m departs from the linear TA model, partially due to the air nonlinear thermal conductivity  $k_g \propto \sqrt{T}$  [13] and the graphene-aerogel nonlinear specific heat below the Debye temperature  $\Theta_D \approx 2100 \text{ K}$  for carbon allotropes [30] (see Sec. II). Furthermore, from Fig. 5 we confirm that by heterodyning, only the sound pressure of the first harmonic is linearly dependent on  $V_{dc}$ , at low power. The nonlinear behavior observed at higher power is due to the nonlinear specific heat of the graphene aerogel. Therefore, it is possible to amplify the SPL of a graphene aerogel by applying a small dc voltage in series with the ac voltage applied to the sample.

In Figs. 6(a) and 6(b), the frequency response of the input (electrical) and output (sound) signals, respectively, is reported in the infrasound (10 Hz), audible (10 kHz), and ultrasound (10 MHz) ranges to evaluate the harmonic distortion of the sound generated by the graphene aerogel. We note no harmonic distortion in graphene aerogels over the range investigated. In our experiments the first-harmonic generation is obtained by heterodyning [22], as a dc voltage is applied in series with the ac voltage to the samples. By comparison, commercial hi-fi loudspeakers and earphones typically have a total harmonic distortion of about 1% [10].

The theoretical and experimental directivity patterns [3] of the sound emitted at 1 W and 1 m from the graphene aerogel are reported in the azimuthal plane [Fig. 7(a)] and the polar plane [Fig. 7(b)]. The samples behave as an omnidirectional point source up to 20 kHz, beyond which they exhibit a multipolar pattern, as shown, for instance, at 1 MHz. Since there are no electromechanically moving parts in the emitter, the sound is equally generated with no destructive interference from both sides of the illuminated spot of the aerogel [10], which acts as a diaphragm of thermal thickness  $\mu \equiv \sqrt{\alpha_s/\pi f} = 0.1 \mu\text{m}$  to 1 mm in the frequency range studied here. Hence, no bass-reflex technique [3] is needed in TA transducers. Moreover, Fig. 7(c) depicts the SPL calculated in space at 1 MHz in the azimuthal plane. The sound is suppressed at given angles

corresponding to the nodes in the directivity pattern in Fig. 7(a).

#### IV. CONCLUSIONS

Graphene aerogels can be effectively used as ultrabroadband TA transducers with omnidirectional emission from 1 Hz to 20 kHz and with no harmonic distortion from 1 Hz to 20 MHz by use of a single, nonmechanically vibrating emitter. For instance, such devices may be improved by use of thicker graphene aerogels with lower electrical impedance to require a lower voltage for operation.

#### ACKNOWLEDGMENTS

The authors acknowledge funding for this work from the European Union's Horizon 2020 research and innovation program under Grant Agreement No. 785219 (GrapheneCore2). The authors also acknowledge that this work has received financial support from the Bilateral Cooperation Agreement between Italy and China of the Italian Ministry of Foreign Affairs and International Cooperation (MAECI) and the National Natural Science Foundation of China in the framework of the project of major relevance entitled "Three-Dimensional Graphene: Applications in Catalysis, Photoacoustics and Plasmonics."

- [1] W. Zhou, J. Vavro, N. M. Nemes, J. E. Fischer, F. Borondics, K. Kamarás, and D. B. Tanner, Charge transfer and Fermi level shift in p-doped single-walled carbon nanotubes, *Phys. Rev. B* **71**, 2054231 (2005).
- [2] H. Tian, C. Li, M. A. Mohammad, Y.-L. Cui, W.-T. Mi, Y. Yanga, D. Xie, and T.-L. Ren, Graphene earphones: Entertainment for both humans and animals, *ACS Nano* **8**, 5883 (2014).
- [3] L. L. Beranek, *Acoustics* (American Institute of Physics, Cambridge, MA, 1993).
- [4] D. B. Kilfoyle and A. B. Baggeroer, The state of the art in underwater acoustic telemetry, *IEEE J. Oceanic Eng.* **25**, 4 (2000).
- [5] F. A. Everest, *Master Handbook of Acoustics* (McGraw-Hill, New York, 2001).
- [6] A. Schnitzler and J. Gros, Normal and pathological oscillatory communication in the brain, *Nat. Rev. Neurosci.* **6**, 285 (2005).
- [7] W. R. Hedrick, D. L. Hykes, and D. E. Starchman, *Ultrasound Physics and Instrumentation* (Elsevier Mosby, Maryland Heights, 2005).
- [8] F. Giorgianni, C. Vicario, M. Shalaby, L. D. Tenuzzo, A. Marcelli, T. Zhang, K. Zhao, Y. Chen, C. Hauri, and S. Lupi, High-efficiency and low distortion photoacoustic effect in 3D graphene sponge, *Adv. Funct. Mater.* **28**, 17026521 (2018).
- [9] P. Guiraud, S. Giordano, O. B. Matar, P. Pernod, and R. Lardat, Two temperature model for thermoacoustic sound generation in thick porous thermophones, *J. Appl. Phys.* **126**, 165111 (2019).
- [10] F. De Nicola, L. D. Tenuzzo, I. Viola, R. Zhang, H. Zhu, A. Marcelli, and S. Lupi, Ultimate photo-thermoacoustic efficiency of graphene aerogels, *Sci. Rep.* **9**, 1 (2019).
- [11] C. S. Kim, K. E. Lee, J.-M. Lee, S. O. Kim, B. J. Cho, and J.-W. Choi, Application of n-doped three-dimensional reduced graphene oxide aerogel to thin film loudspeaker, *ACS Appl. Mater. Interfaces* **8**, 22295 (2016).
- [12] W. Fei, J. Zhou, and W. Guo, Low-voltage driven graphene foam thermoacoustic speaker, *Small* **11**, 2252 (2015).
- [13] A. E. Aliev, N. K. Mayo, M. J. de Andrade, R. O. Robles, S. Fang, R. H. Baughman, M. Zhang, Y. Chen, J. A. Lee, and S. J. Kim, Alternative nanostructures for thermophones, *ACS Nano* **9**, 4743 (2015).
- [14] H. Tian, T.-L. Ren, D. Xie, Y.-F. Wang, C.-J. Zhou, T.-T. Feng, D. Fu, Y. Yang, P.-G. Peng, L.-G. Wang, and L.-T. Liu, Graphene-on-paper sound source devices, *ACS Nano* **5**, 4878 (2011).
- [15] H. Tian, D. Xie, Y. Yang, T.-L. Ren, Y.-F. Wang, C.-J. Zhou, P.-G. Peng, L.-G. Wang, and L.-T. Liu, Single-layer graphene sound-emitting devices: Experiments and modeling, *Nanoscale* **4**, 2272 (2012).
- [16] J. W. Suk, K. Kirk, Y. Hao, N. A. Hall, and R. S. Ruoff, Thermoacoustic sound generation from monolayer graphene for transparent and flexible sound sources, *Adv. Mater.* **24**, 6342 (2012).
- [17] S. C. Xu, B. Y. Man, S. Z. Jiang, C. S. Chen, C. Yang, M. Liu, X. G. Gao, Z. C. Sun, and C. Zhang, Flexible and transparent graphene-based loudspeakers, *Appl. Phys. Lett.* **102**, 1519021 (2013).
- [18] H. Tian, Y. Yang, D. Xie, Y.-L. Cui, W.-T. Mi, Y. Zhang, and T.-L. Ren, Wafer-scale integration of graphene-based electronic, optoelectronic and electroacoustic devices, *Sci. Rep.* **4**, 35981 (2014).
- [19] Y. Tian, H. Tian, Y. L. Wu, L. L. Zhu, L. Q. Tao, W. Zhang, Y. Shu, D. Xie, Y. Yang, Z. Y. Wei, X. H. Lu, T.-L. Ren, C.-K. Shih, and J. Zhao, Coherent generation of photo-thermoacoustic wave from graphene sheets, *Sci. Rep.* **5**, 105821 (2015).
- [20] C. S. Kim, S. K. Hong, J.-M. Lee, D.-S. Kang, B. J. Cho, and J.-W. Choi, Free-standing graphene thermophone on a polymer-mesh substrate, *Small* **12**, 185 (2016).
- [21] L.-Q. Tao, H. Tian, Y. Liu, Z.-Y. Ju, Y. Pang, Y.-Q. Chen, D.-Y. Wang, X.-G. Tian, J.-C. Yan, N.-Q. Deng, Y. Yang, and T.-L. Ren, An intelligent artificial throat with sound-sensing ability based on laser induced graphene, *Nat. Commun.* **8**, 145791 (2017).
- [22] M. S. Heath and D. W. Horsell, Multi-frequency sound production and mixing in graphene, *Sci. Rep.* **7**, 13631 (2017).
- [23] V. Vesterinen, A. O. Niskanen, J. Hassel, and P. Heliö, Fundamental efficiency of nanothermophones: Modeling and experiments, *Nano Lett.* **10**, 5020 (2010).
- [24] H. Hu, T. Zhu, and J. Xu, Model for thermoacoustic emission from solids, *Appl. Phys. Lett.* **96**, 2141011 (2010).
- [25] T. Kihara, T. Harada, M. Kato, K. Nakano, O. Murakami, T. Kikusui, and N. Koshida, Reproduction of mouse-pup ultrasonic vocalizations by nanocrystalline silicon thermoacoustic emitter, *Appl. Phys. Lett.* **88**, 043902 (2006).



- [26] T. L. Szabo, *Diagnostic Ultrasound Imaging: Inside Out* (Academic Press, Cambridge, 2004).
- [27] T. Awad, H. Moharram, O. Shaltout, D. Asker, and M. Youssef, Applications of ultrasound in analysis, processing and quality control of food: A review, *Food Res. Int.* **48**, 410 (2012).
- [28] F. De Nicola, I. Viola, L. D. Tenuzzo, F. Rasch, M. R. Lohe, A. S. Nia, F. Schütt, X. Feng, R. Adelung, and S. Lupi, Wetting properties of graphene aerogels, *Sci. Rep.* **10**, 1 (2020).
- [29] H. B. Callen, *Thermodynamics and an Introduction to Thermostatistics* (John Wiley & Sons, New York, 1985).
- [30] E. Pop, V. Varshney, and A. K. Roy, Thermal properties of graphene: Fundamentals and applications, *MRS Bull.* **37**, 1273 (2012).
- [31] W. J. Parker, R. J. Jenkins, C. P. Butler, and G. L. Abbott, Flash method of determining thermal diffusivity, heat capacity, and thermal conductivity, *J. Appl. Phys.* **32**, 1679 (1961).
- [32] A. E. Aliev, M. D. Lima, S. Fang, and R. H. Baughman, Underwater sound generation using carbon nanotube projectors, *Nano Lett.* **10**, 2374 (2010).
- [33] D. T. Blackstock, *Fundamentals of Physical Acoustics* (John Wiley & Sons, New York, 2000).